Electronic Supplementary Information (ESI) for: Can Oppositely Charged Polyelectrolyte Stars Form a Gel? A Simulational Study

Andrea Tagliabue,[†] Jonas Landsgesell,[‡] Massimo Mella,[†] and Christian Holm[*,‡]

[†]*Dipartimento di Scienza ed Alta Tecnologia, Università degli Studi dell'Insubria, via Valleggio 9, 22100, Como, Italy*

[‡]*Institute for Computational Physics, University of Stuttgart, Allmandring 3, Stuttgart, 70569, Germany*

E-mail: holm@icp.uni-stuttgart.de

Methods

In this section we discuss in detail the computational protocol implemented to compute τ_{bond} and to detect the ionic bond dissociation/formation mechanisms discussed in the main text.

At each time $t = t_0$, we define a "contact matrix" $\mathbb{H}_{\mathrm{a}}(t_0)$ as

$$\mathbb{H}_{\mathrm{a}}(t_0) = \begin{bmatrix} h_{11} & \dots & h_{1n} \\ h_{21} & \dots & h_{2n} \\ \dots & \dots & \dots \\ h_{m1} & \dots & h_{mn} \end{bmatrix} \tag{1}$$

Each element $h_{\alpha\beta}$ (with $\alpha = 1, 2, \dots, m$, where m is the total number of positively charged chains; and $\beta = 1, 2, \dots, n$, where n is the total number of negatively charged chains) is a

binary variable that is equal to 1 if the two chains α and β are in contact with each other, and it is 0 otherwise. Computing $\mathbb{H}_{\rm a}(t_0 = 0)$ and repeating process at regular time intervals $\Delta\tau$ allow us to build a 3D matrix $\mathbb{H}_{\rm a}(t, \alpha, \beta) = \mathbb{H}_{\rm a}$ (with size $\frac{t_{\rm sim}}{\Delta\tau} \times m \times n$) that contains all the information about the time evolution of all the contacts. Thus, from $\mathbb{H}_{\rm a}$ it is possible to compute the following structural properties at the time t_0:

- the number of contacts for a given arm α:

$$\eta_{{\rm a},\alpha}(t_0) = \sum_{\beta=1}^{n} h_{t_0\alpha\beta}. \tag{2}$$

- the fraction of dangling arms at a certain time t_0,

$$\Delta_{\rm a}(t_0) = \frac{1}{n+m}\left[\sum_{\alpha=1}^{m}\delta\left(\sum_{\beta=1}^{n} h_{t_0\alpha\beta}\right) + \sum_{\beta=1}^{n}\delta\left(\sum_{\alpha=1}^{m} h_{t_0\alpha\beta}\right)\right], \tag{3}$$

  where $\delta(x)$ is a function that returns 1 if $x = 0$, and 0 otherwise. Hence, $\Delta_{\rm a}(t_0)$ corresponds to the number of null rows plus the number of null columns of $\mathbb{H}_{\rm a}(t_0)$;

It is evident that is possible to build a similar matrix in order to analyse the contacts between stars, i.e. $\mathbb{H}_{\rm s}(t, A, B) = \mathbb{H}_{\rm s}$, where $A = 1, 2, \ldots, M$ and $B = 1, 2, \ldots, N$; here, M and N are the total number of positive and negative stars, respectively. Thus, it immediately follows that from $\mathbb{H}_{\rm s}$ it is possible to calculate the number of isolated stars in solutions ($\Delta_{\rm s}$) and the number of contacts for a given star A ($\eta_{{\rm s},A}$) in a similar way to what is done for the analogous properties of arms.

We also define the matrix $\mathbb{J}_{\rm a}$ at the time $t = t_0 + \Delta\tau$ as

$$\mathbb{J}_{\rm a}(t_0 + \Delta\tau) = \mathbb{H}_{\rm a}(t_0 + \Delta\tau) - \mathbb{H}_{\rm a}(t_0) = \begin{bmatrix} j_{11} & \cdots & j_{1n} \\ j_{21} & \cdots & j_{2n} \\ \cdots & \cdots & \cdots \\ j_{m1} & \cdots & j_{mn} \end{bmatrix} \tag{4}$$

In this case, $j_{\alpha\beta}$ is a variable that can assume three different values: $j_{\alpha\beta} = 1$ if a contact between two arms α and β is formed in the time interval $(t_0, t_0 + \Delta\tau]$; $j_{\alpha\beta} = -1$ if a pre–existing contact between two arms α and β broke in the interval $(t_0, t_0 + \Delta\tau]$; and $j_{\alpha\beta} = 0$ otherwise. For two generic ionically bonded chains α and β, the contact time $\tau_{\rm bond}$ can be easily computed from $\mathbb{J}_{\rm a}$ identifying the time-frames at which the contact forms ($t_{\rm f}$, $j_{t_{\rm f}\alpha\beta} = 1$) and breaks ($t_{\rm b}$, $j_{t_{\rm b}\alpha\beta} = -1$), so that $\tau_{\rm bond} = t_{\rm b} - t_{\rm f}$. From $\mathbb{J}_{\rm a}$ one can easily define, for a certain time $t = t_0$ and for a given arm α, the set of other chain in contact with α, the set of contacts formed by α in the time interval $(t_0, t_0 + \Delta\tau]$, and the set of contacts lost by α in the interval $(t_0, t_0 + \Delta\tau]$. We call these sets $\mathbb{L}_{\rm f}(t_0, \alpha)$, $\mathbb{L}_{\rm b}(t_0, \alpha)$, $\mathbb{L}_{\rm c}(t_0, \alpha)$, respectively.

The mechanisms that could lead to the network restructuring are: (a) "intermittent bond", $\mathcal{I}$; (b) "anticipated partner switch", $\mathcal{S}_{\rm ant}$; and (c) "postponed partner switch", $\mathcal{S}_{\rm pos}$. Here we discuss more in detail these three mechanisms and the rules implemented to categorize the contact formation/dissociation events.

"intermittent contact" ($\mathcal{I}$)

We classify as "intermittent" a contact that, after lasting in solution for a time $\tau_{\rm bond}$, it temporally breaks and then it reforms after a time $\tau_{\rm lag}$ (see Figure S1 (a)). It can be described by the following equation:

$$\alpha\cdots\beta \underset{\tau_{\rm lag}}{\overset{\tau_{\rm bond}}{\rightleftarrows}} \alpha + \beta. \tag{5}$$

Thus, it consists of three sub–events: (i) contact formation at time $t_{\rm f}$; (ii) contact breaking at time $t_{\rm b}$; and (iii) contact re–formation at time $t'_{\rm f}$. It follows that $\tau_{\rm bond} = t_{\rm b} - t_{\rm f}$ and $\tau_{\rm lag} = t'_{\rm f} - t_{\rm b}$. The set of rules implemented to detect this type of event is:

1) $t_{\rm f} < t_{\rm b} < t'_{\rm f}$;

2) $\#\mathbb{L}_{\rm f}(t, \alpha) = 1$, $\#\mathbb{L}_{\rm b}(t, \alpha) = 0$ for $t = t_{\rm f}$, $t'_{\rm f}$ ("#" denotes the cardinality of the set);

3) $\#\mathbb{L}_{\rm f}(t, \alpha) = 0$, $\#\mathbb{L}_{\rm b}(t, \alpha) = 1$ for $t = t_{\rm b}$;

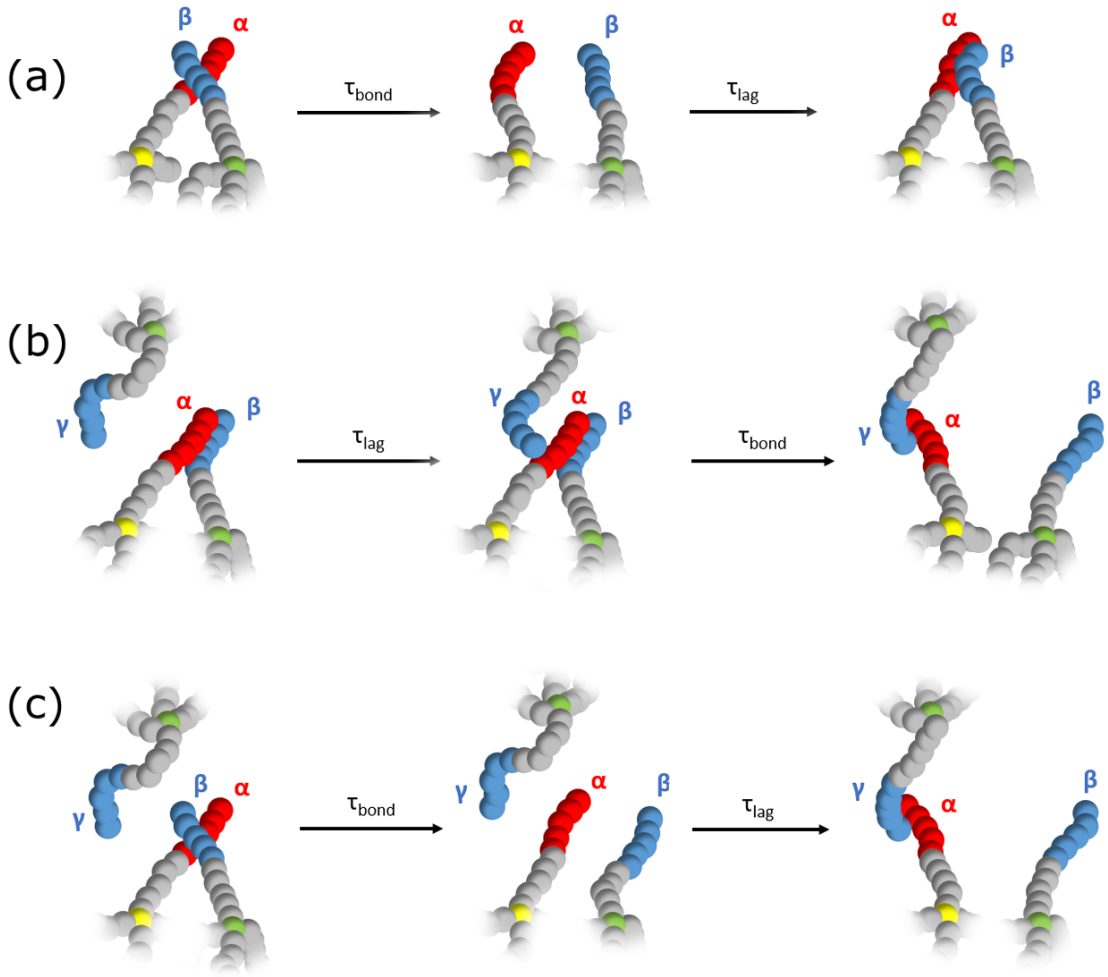

Figure S1: Pictorial description of the three analysed mechanisms: (a) $\mathcal{I}$; (b) $\mathcal{S}_{\text{ant}}$; (c) $\mathcal{S}_{\text{pos}}$.

4) $\sum_{t=t_\mathrm{f}+\Delta\tau}^{t_\mathrm{b}-\Delta\tau} \#\mathbb{L}_\mathrm{f}(t,\alpha) - \sum_{t=t_\mathrm{f}+\Delta\tau}^{t_\mathrm{b}-\Delta\tau} \#\mathbb{L}_\mathrm{b}(t,\alpha) = 0$;

5) $\sum_{t=t_\mathrm{b}+\Delta\tau}^{t'_\mathrm{f}-\Delta\tau} \#\mathbb{L}_\mathrm{f}(t,\alpha) = 0$;

6) $\mathbb{L}_\mathrm{f}(t_\mathrm{f},\alpha) = \mathbb{L}_\mathrm{f}(t'_\mathrm{f},\alpha)$;

In other words, item 1) establishes the time sequence of the sub–events; items 2) and 3) states that no other contact formations/ruptures are allowed to taking place at times t_f, t'_f, and t_b); item 4) states that no net gain/lost of contacts is allowed in the time interval $(t_\mathrm{f}, t_\mathrm{b})$; item 5) states that no other contact can be formed between t_b and t'_f; finally, item 6) checks that α get in touch with the same chain β at t_f and t'_f.

"postponed partner switch" ($\mathcal{S}_\mathrm{pos}$)

We classify as "postponed partner switch" an event that is described by the following equation:

$$\gamma + \alpha\cdots\beta \xrightarrow{\tau_\mathrm{bond}} \gamma + \alpha + \beta \xrightarrow{\tau_\mathrm{lag}} \gamma\cdots\alpha + \beta. \tag{6}$$

Hence, it consists in three sub–events: (i) $\alpha\cdots\beta$ contact formation at time t_f; (ii) $\alpha\cdots\beta$ contact breaking at time t_b; and (iii) $\alpha\cdots\gamma$ contact formation at time t'_f, with $\beta \neq \gamma$ (see Figure S1 (c)) As for the $\mathcal{I}$ case, $\tau_\mathrm{bond} = t_\mathrm{b} - t_\mathrm{f}$ and $\tau_\mathrm{lag} = t'_\mathrm{f} - t_\mathrm{b}$. The set of rules describing the "postponed partner switch" is the same as those that describe an "intermittent contact", with the exception of item 6) that reads:

6) $\mathbb{L}_\mathrm{f}(t_\mathrm{f},\alpha) \neq \mathbb{L}_\mathrm{f}(t'_\mathrm{f},\alpha)$.

"anticipated partner switch" ($\mathcal{S}_\mathrm{pos}$)

Finally, we classify as "anticipated partner switch" those events in which the dissociation of a contact $\alpha\cdots\beta$ is preceded by the formation of a contact $\alpha\cdots\gamma$ (see Figure S1 (b)); that is

$$\gamma + \alpha\cdots\beta \xrightarrow{\tau_\mathrm{lag}} \gamma\cdots\alpha\cdots\beta \xrightarrow{\tau_\mathrm{bond}} \gamma\cdots\alpha + \beta. \tag{7}$$

Once again, the event consists in three sub–events: (i) $\alpha \cdots \beta$ contact formation at time t_{f}; (ii) $\alpha \cdots \gamma$ contact formation at time t'_{f}; and (iii) $\alpha \cdots \gamma$ contact breaking at time t'_{f}. Notice that in this case $t'_{\mathrm{f}} < t_{\mathrm{b}}$, so that $\tau_{\mathrm{lag}} = t'_{\mathrm{f}} - t_{\mathrm{f}}$ and $\tau_{\mathrm{bond}} = t_{\mathrm{b}} - t'_{\mathrm{f}}$. Thus, the rules implemented to identify these events are:

1) $t_{\mathrm{f}} < t'_{\mathrm{f}} < t_{\mathrm{b}}$;

2) $\#\mathbb{L}_{\mathrm{f}}(t, \alpha) = 1$, $\#\mathbb{L}_{\mathrm{b}}(t, \alpha) = 0$ for $t = t_{\mathrm{f}}, t'_{\mathrm{f}}$;

3) $\#\mathbb{L}_{\mathrm{f}}(t, \alpha) = 0$, $\#\mathbb{L}_{\mathrm{b}}(t, \alpha) = 1$ for $t = t_{\mathrm{b}}$;

4) $\sum_{t=t_{\mathrm{f}}+1}^{t'_{\mathrm{f}}-1} \#\mathbb{L}_{\mathrm{f}}(t, \alpha) = \sum_{t=t'_{\mathrm{f}}+1}^{t_{\mathrm{b}}-1} \#\mathbb{L}_{\mathrm{f}}(t, \alpha) = 0$;

We classify all those mechanisms that cannot be included in those three categories as "other mechanisms" ($\mathcal{O}$). Let us stress that $\Delta\tau$ plays a fundamental role in classifying the mechanisms due to the fact that the algorithm is not able to discern the temporal order of two (or more) sub–events that take place in the same time interval $[t_0, t + \Delta\tau]$ (*vide infra* Figure S13).

Results: Properties of Single Stars

In order to investigate star conformational properties as a function of the number of their terminal charges, we simulated a single star in condition of very high dilution for each Ω value[1]. We computed the average star radius of gyration R_{G}, where

$$\langle R_{\mathrm{G}}^2 \rangle = \frac{\langle \sum_i^{N_{\mathrm{mono}}^{(\mathrm{s})}} |\mathbf{r}_{\mathrm{CoM}} - \mathbf{r}_i|^2 \rangle}{N_{\mathrm{mono}}^{(\mathrm{s})}}, \tag{8}$$

$\mathbf{r}_i$ and $\mathbf{r}_{\mathrm{CoM}}$ are, respectively, the position vector of the i-th particle and the position vector of the star's center of mass, and $N_{\mathrm{mono}}^{(\mathrm{s})} = 41$ is the number of monomers composing the polyelectrolyte. We also calculated the average star hydrodynamic radius R_{H}, where

$$\left\langle \frac{1}{R_{\mathrm{H}}} \right\rangle = \frac{\langle \sum_{i,\, j>i}^{N_{\mathrm{mono}}^{(\mathrm{s})}} \frac{1}{r_{ij}} \rangle}{(N_{\mathrm{mono}}^{(\mathrm{s})})^2}; \tag{9}$$

where r_{ij} is the distance between the monomers i and j. Finally, we computed the "root mean square arms extension" d_{a},

$$\langle d_{\mathrm{a}} \rangle = \sqrt{\langle |\mathbf{r}_{\mathrm{nuc}} - \mathbf{r}_{\mathrm{last},\alpha}|^2 \rangle}, \tag{10}$$

where $\mathbf{r}_{\mathrm{nuc}}$ and $\mathbf{r}_{\mathrm{last},\alpha}$ are the position vectors of the star nucleus and of the last monomer of the arm α of a given star, respectively. Results are reported in Table S1. As expected, the value of all properties increases with the number of terminal charges carried by the polyelectrolyte.

[1]In practice, for each Ω value we simulated in a very large box a pair of oppositely charged stars kept separated one to each other by fixing their central beads ad a distance larger then 100σ

Table S1: Single star conformational properties as a function of Ω. The neutral case ($\Omega = 0$) is also shown for comparison. The numbers in brackets indicate the statistical error in the last significant digit.

Ω	**0**	**1**	**2**	**3**	**4**	**5**
$\langle R_{\mathrm{G}} \rangle$ (σ)	3.30(1)	3.34(1)	3.51(1)	3.69(1)	4.01(1)	4.24(1)
$\langle R_{\mathrm{H}} \rangle$ (σ)	6.54(1)	6.58(1)	6.82(1)	7.06(1)	7.42(1)	7.75(1)
$\langle d_{\mathrm{a}} \rangle$ (σ)	5.20(3)	5.10(3)	5.33(3)	5.84(4)	6.12(3)	6.76(3)

Results: Determining the Free–Swelling Equilibrium

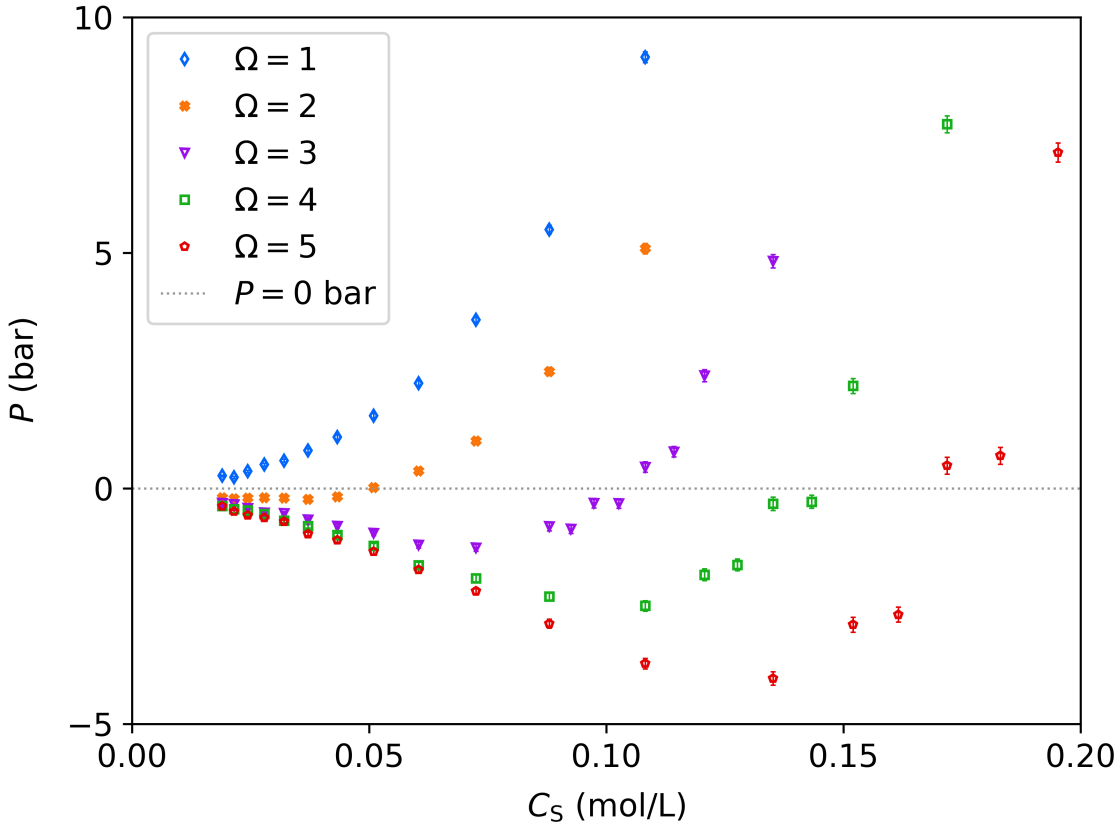

Figure S2: Volume averaged virial pressure P (bar) as a function of the species concentration C_S (mol/L) for the four Ω values. The dotted grey line is only a guide for the eye for discern positive and negative pressure values. Standard error bars are smaller than plot symbols where they are not visible.

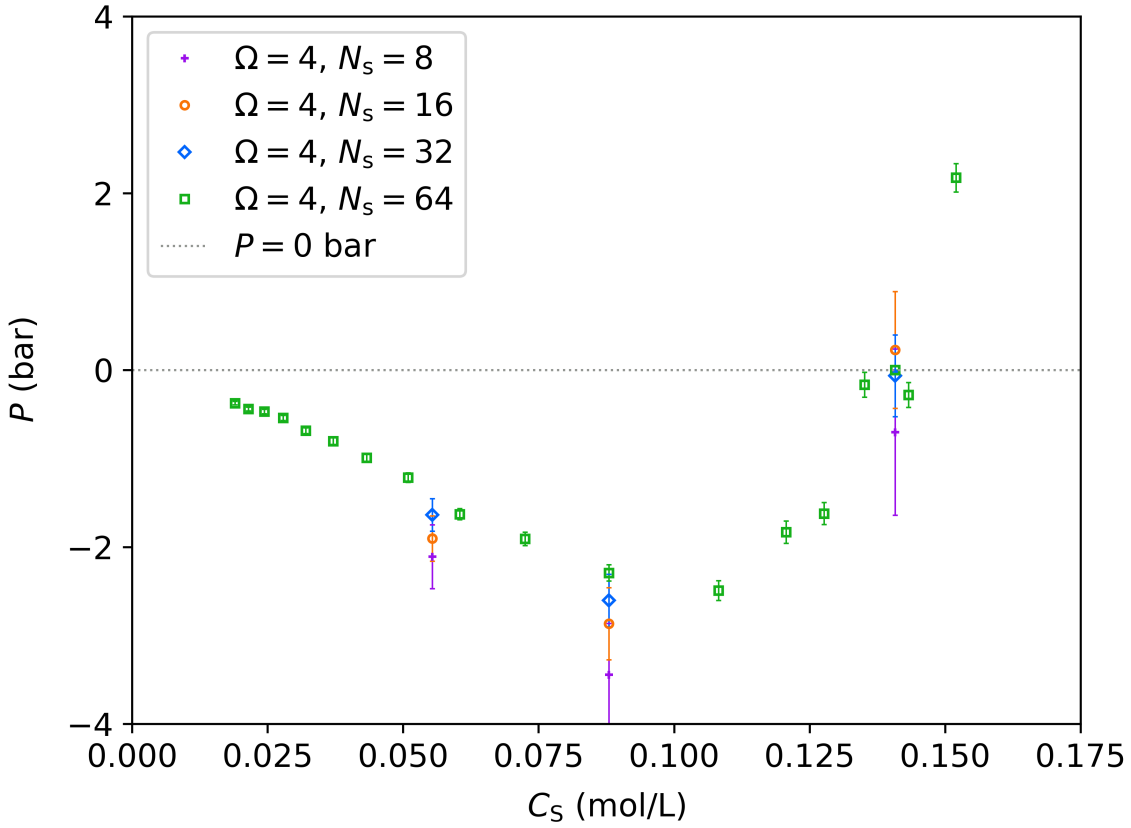

Figure S3: Volume averaged virial pressure P (bar) as a function of the species concentration C_S (mol/L) for the four Ω values. The dotted grey line is only a guide for the eye for discern positive and negative pressure values.

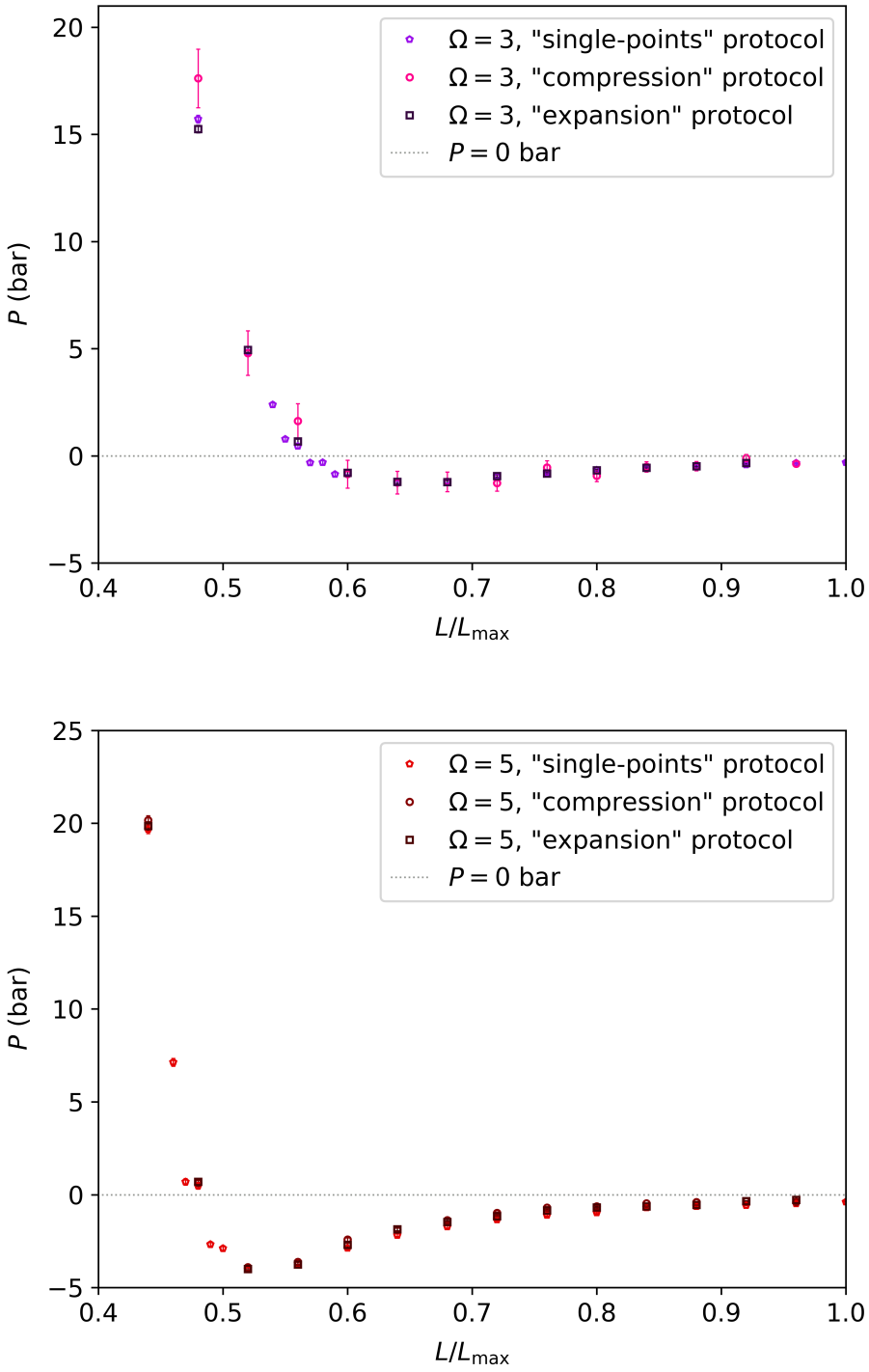

Figure S4: Comparison between the results obtained via the three different simulation protocols described in Section 2.2 for the $\Omega = 3$ and 5 cases (upper and lower panel, respectively). The dotted grey line is only a guide for the eye for discern positive and negative pressure values. Standard error bars are smaller than plot symbols where they are not visible.

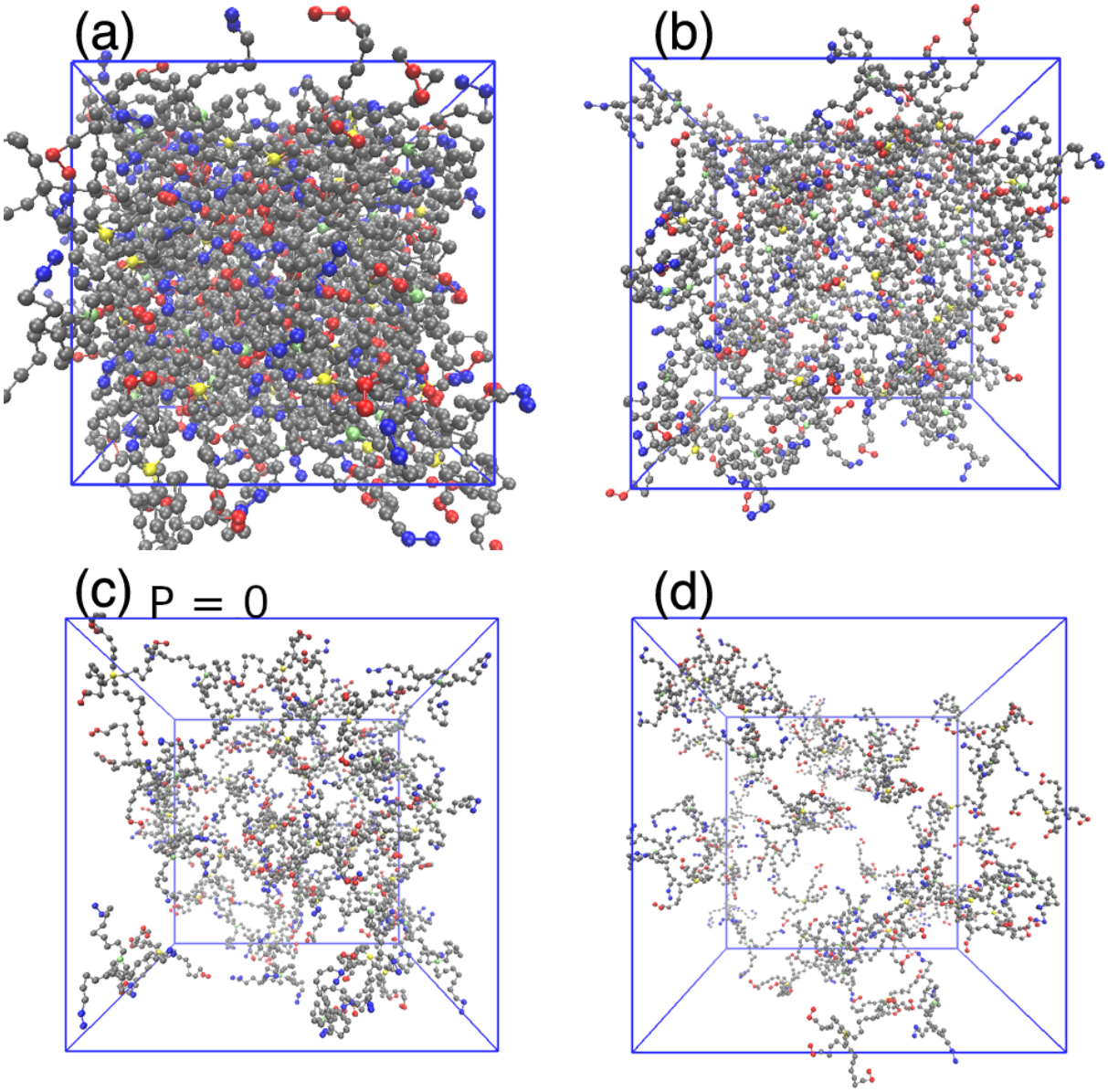

Figure S5: Trajectory snapshots for $\Omega = 2$ taken at different box length values: (a) $L = 16\sigma$, $L/L_{\max} = 0.36$; (b) $L = 26\sigma$, $L/L_{\max} = 0.56$; (c) $L = 36\sigma$, $L/L_{\max} = 0.72$, $P = 0$; (d) $L = 48\sigma$, $L/L_{\max} = 0.96$. The diameter of all monomers has been reduced by roughly one half with respect to the real one in order to improve the clarity of the pictures.

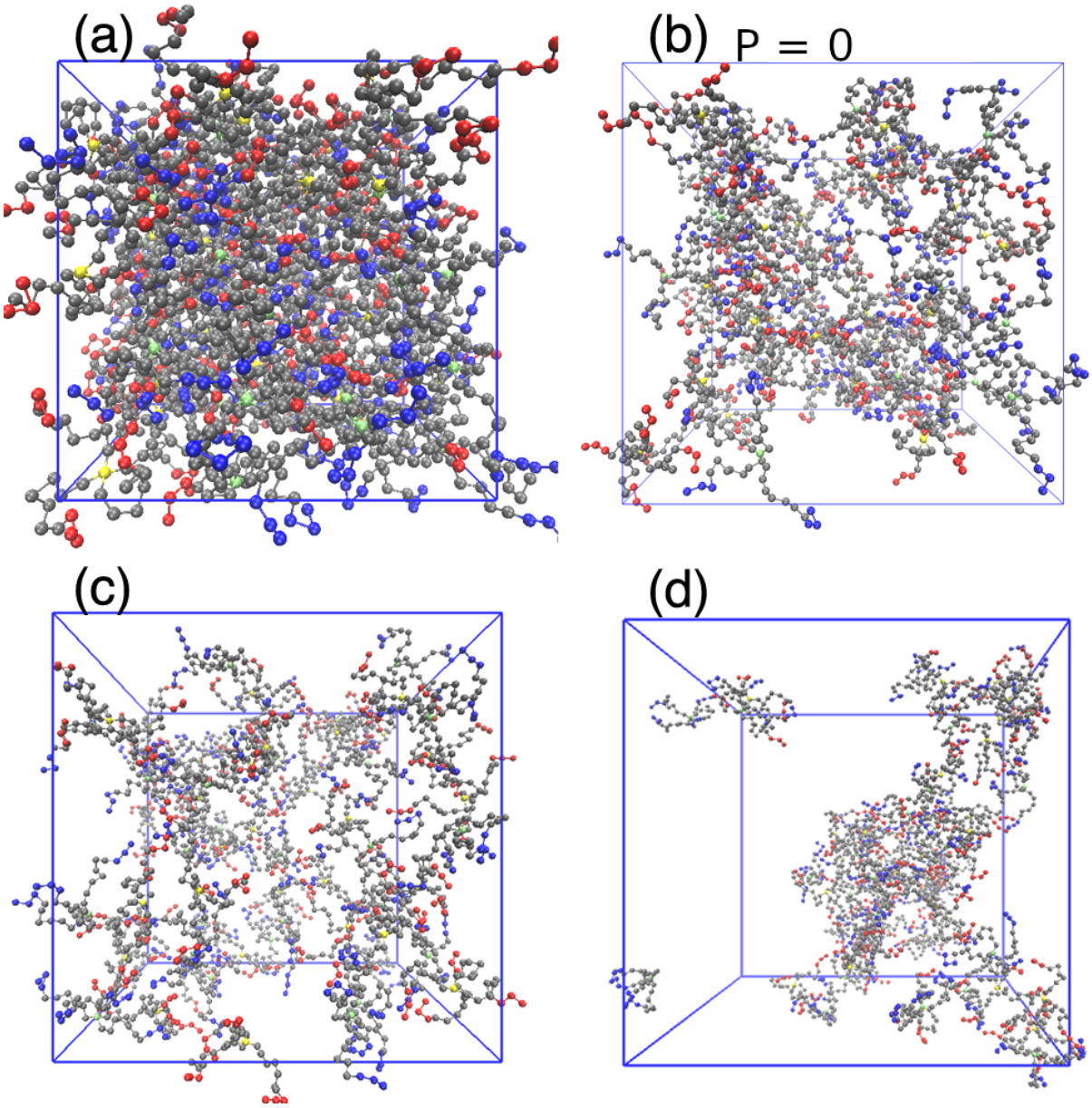

Figure S6: Trajectory snapshots for $\Omega = 3$ taken at different box length values: (a) $L = 18\sigma$, $L/L_{\max} = 0.36$; (b) $L = 28.27\sigma$, $L/L_{\max} = 0.56$, $P = 0$; (c) $L = 34\sigma$, $L/L_{\max} = 0.68$; (d) $L = 48\sigma$, $L/L_{\max} = 0.96$. The diameter of all monomers has been reduced by roughly one half with respect to the real one in order to improve the clarity of the pictures.

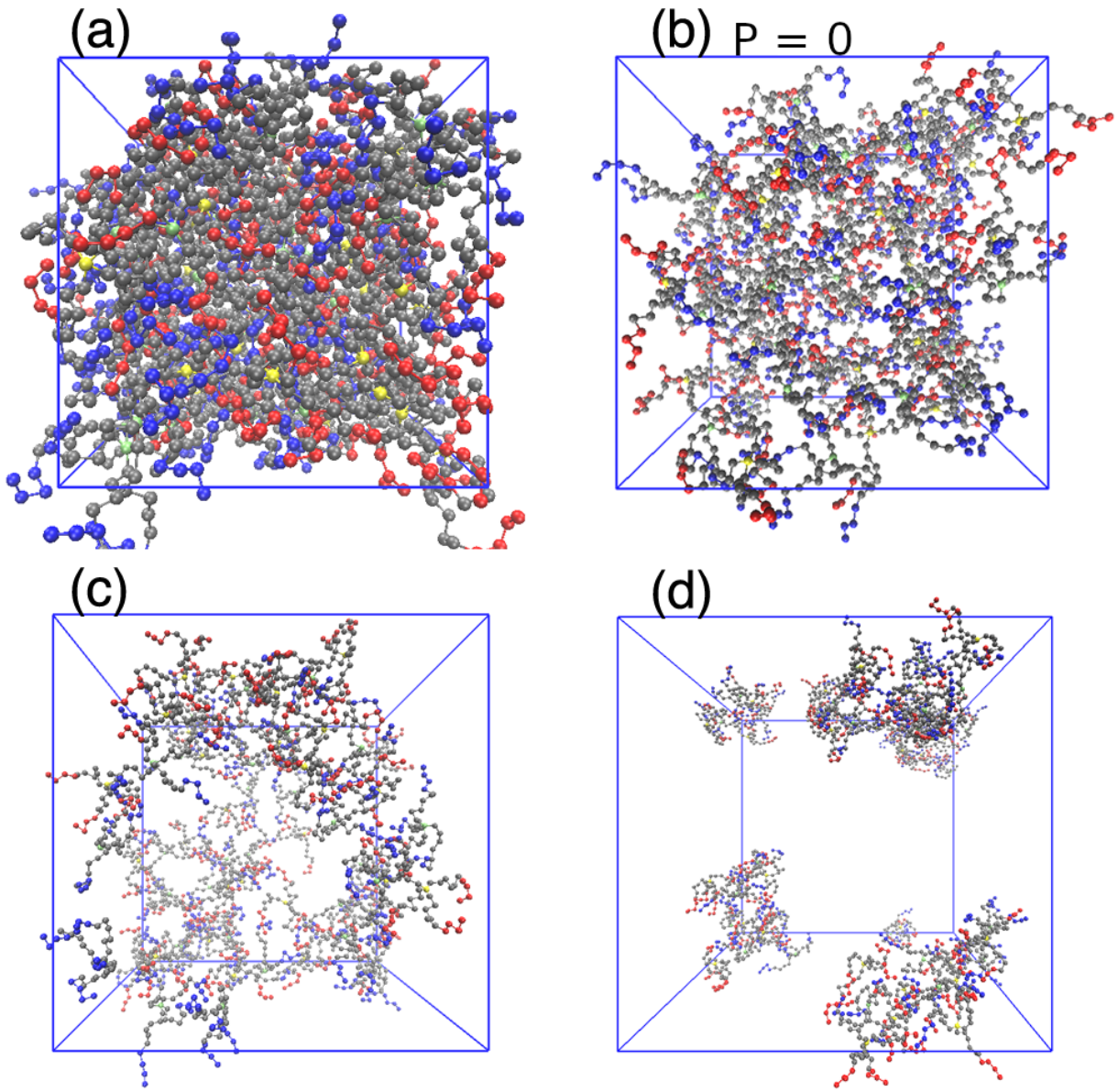

Figure S7: Trajectory snapshots for $\Omega = 4$ taken at different box length values: (a) $L = 16\sigma$, $L/L_{\max} = 0.36$; (b) $L = 25.65\sigma$, $L/L_{\max} = 0.51$, $p \simeq 0$; (c) $L = 36\sigma$, $L/L_{\max} = 0.72$; (d) $L = 48\sigma$, $L/L_{\max} = 0.96$. The diameter of all monomers has been reduced by roughly one half with respect to the real one in order to improve the clarity of the pictures.

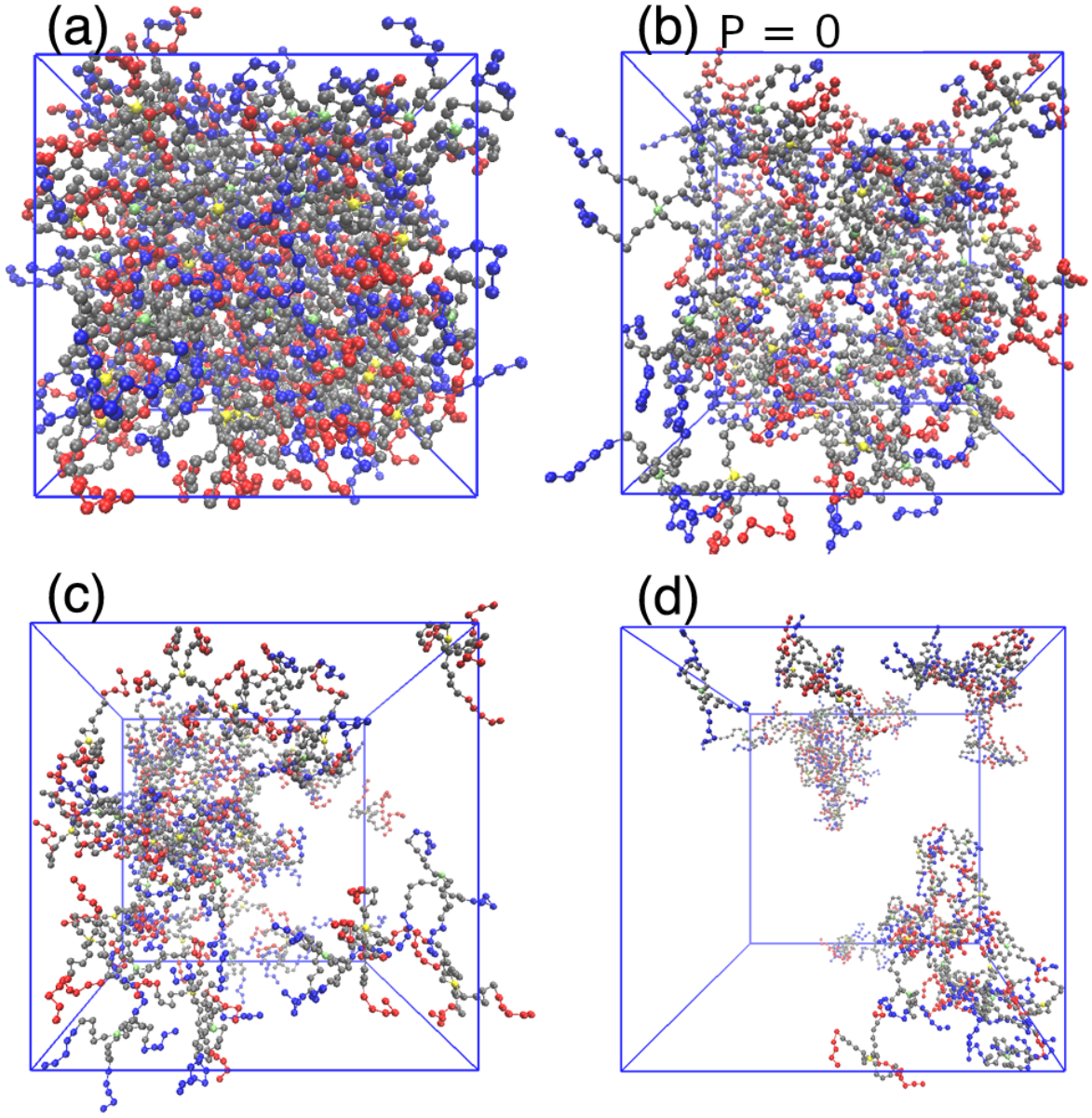

Figure S8: Trajectory snapshots for $\Omega = 5$ taken at different box length values: (a) $L = 18\sigma$, $L/L_{\max} = 0.36$; (b) $L = 23.84\sigma$, $L/L_{\max} = 0.48$, $P = 0$; (c) $L = 34\sigma$, $L/L_{\max} = 0.68$; (d) $L = 48\sigma$, $L/L_{\max} = 0.96$. The diameter of all monomers has been reduced by roughly one half with respect to the real one in order to improve the clarity of the pictures.

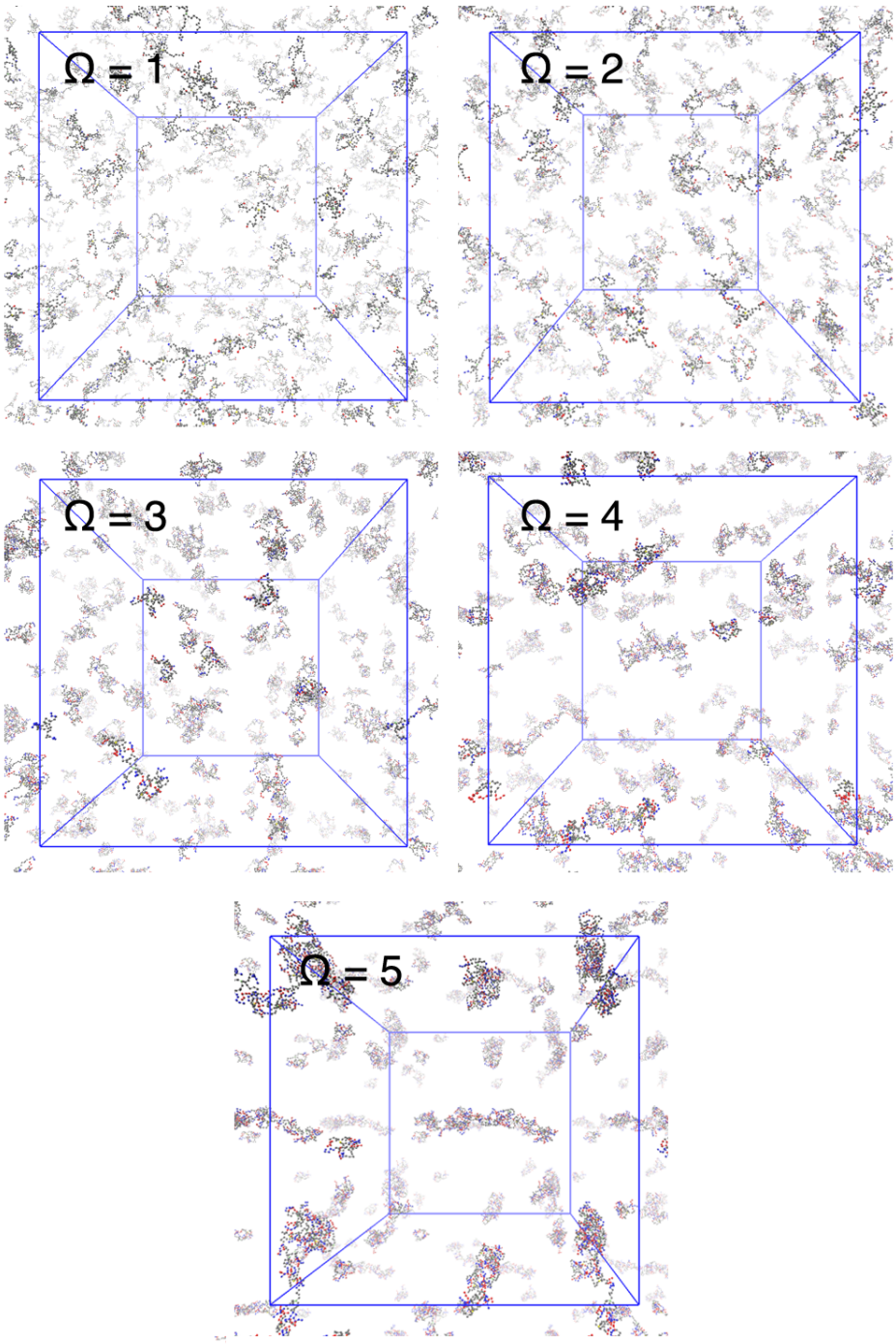

Figure S9: Trajectory snapshots for different Ω values taken at box length $L = 95\sigma$ ($L/L_{\max} = 1.90$, $C_S = 1.38 \cdot 10^{-3}$ mol/L). Periodic boundary conditions replicas are shown in some directions. The diameter of all monomers has been reduced by roughly one half with respect to the real one in order to improve the clarity of the pictures.

Results: Structural Properties at the Free–Swelling Equilibrium

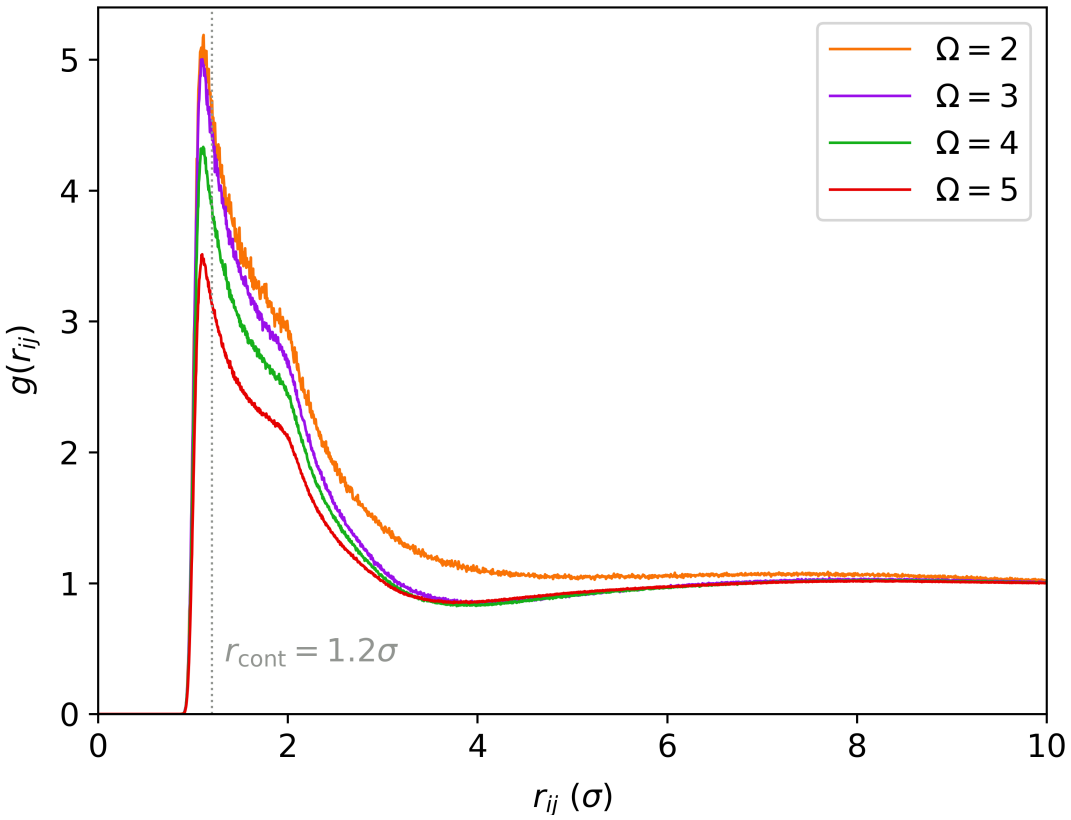

Figure S10: Pair distribution functions calculated between positively and negatively charged monomer. The grey dotted vertical line indicates the value of the cutoff radius r_{cont} used to define a "contact" between two oppositely charged stars (or arms).

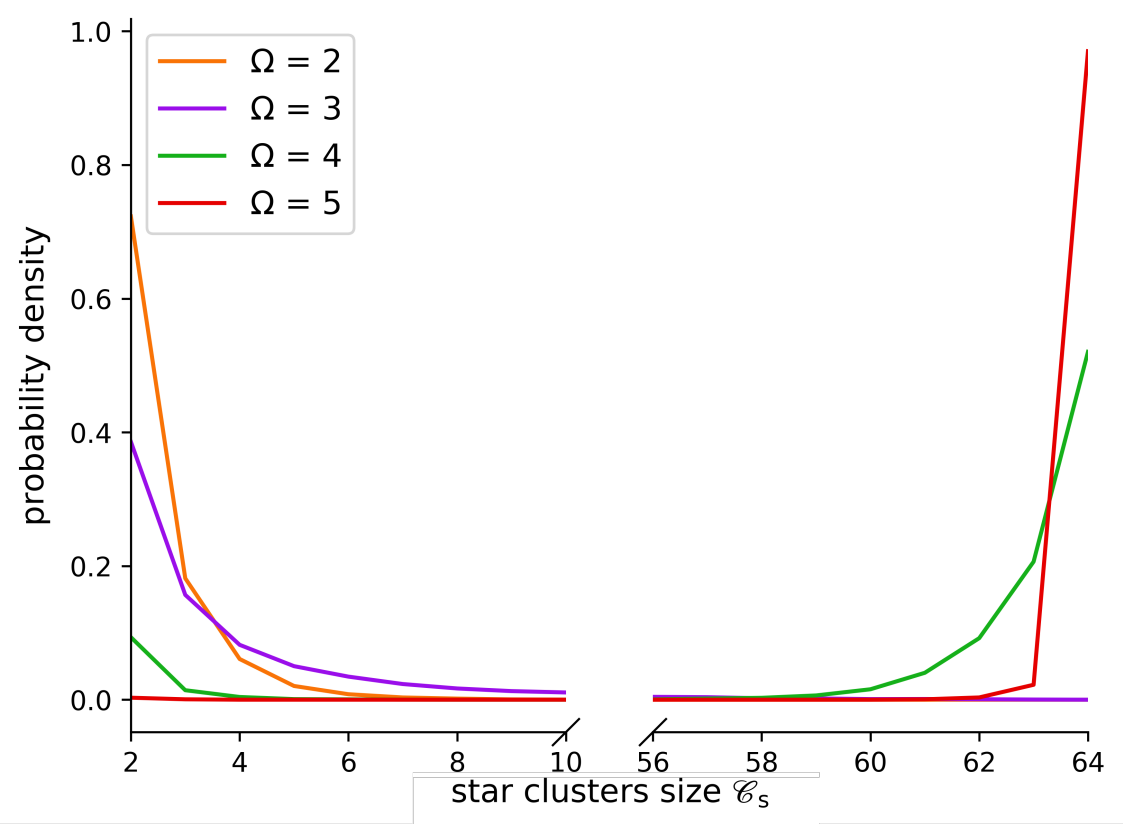

Figure S11: Probability density to find a CoS with a certain size $\mathscr{C}_s$ in solution for the four Ω values.

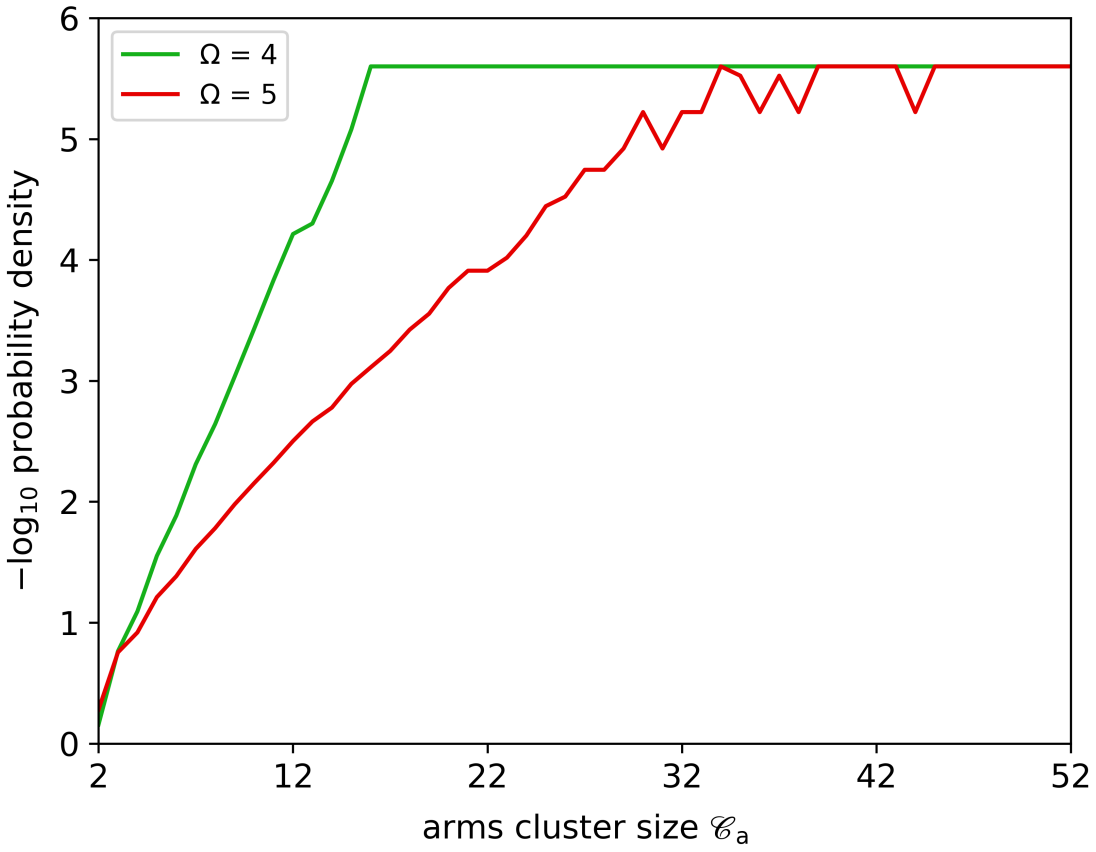

Figure S12: $-\log_{10}$ of the probability density to observe a chain belonging to a CoA of size $\mathscr{C}_a$ for $\Omega = 4$ and 5. In case of 0 occurrences of clusters with a certain size $\mathscr{C}_a$, we arbitrary set the $-\log_{10}$ of the probability density to 5.6.

Results: Ionic Bond Lifetimes

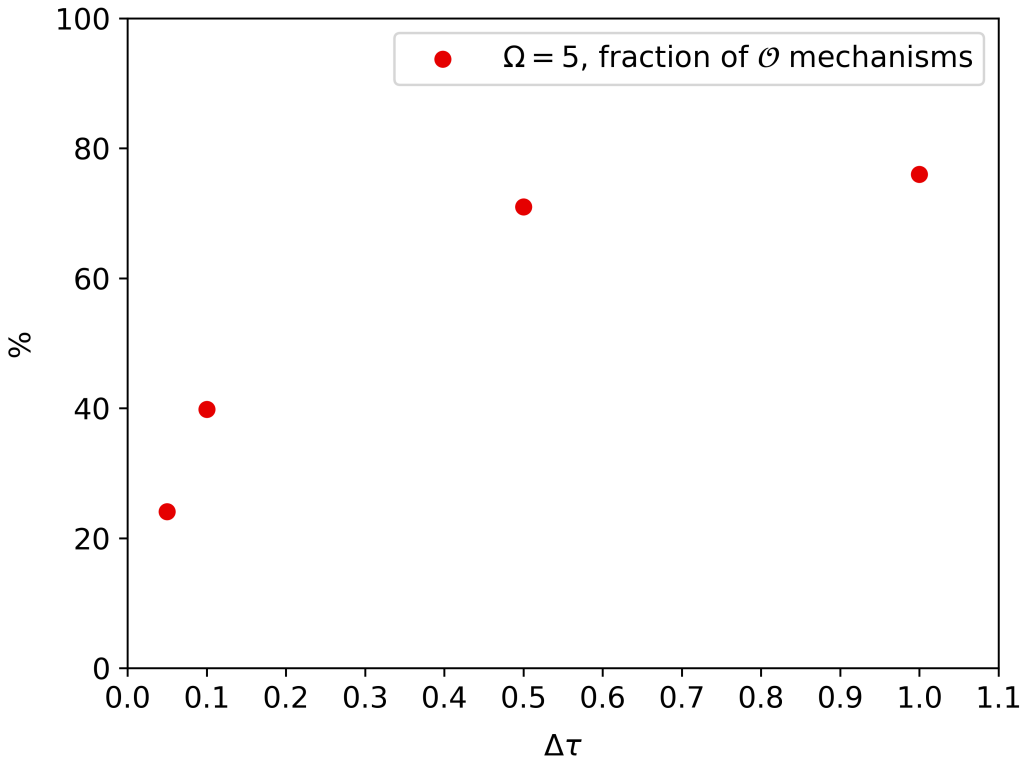

Figure S13: Fraction of non–classifiable mechanisms ($\mathcal{O}$) as a function of the time resolution $\Delta\tau$ for the $\Omega = 5$ case.

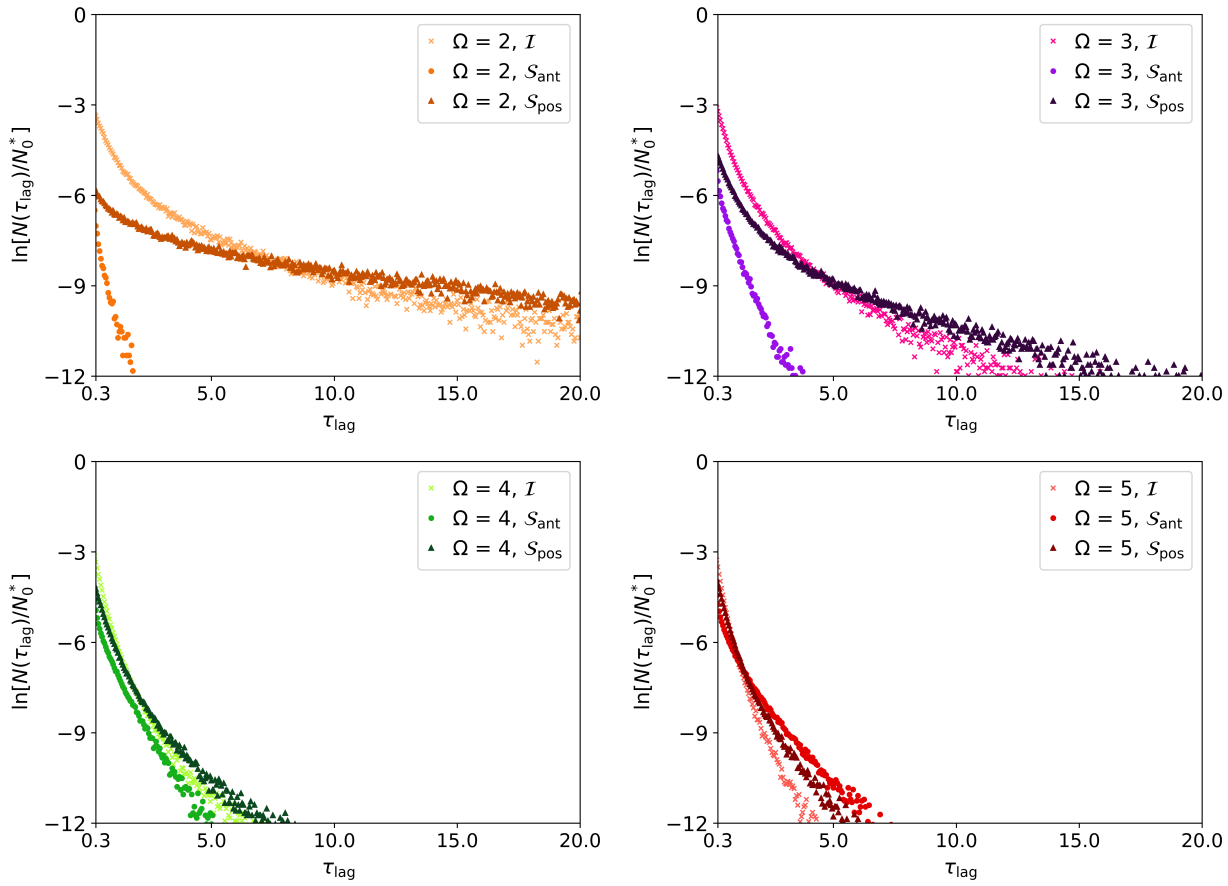

Figure S14: Natural logarithm of $N(t)/N_0^*$ versus τ_{lag} (system time units) for the three mechanisms at the four Ω values. N_0^* is the number of contacts that have just dissociated.

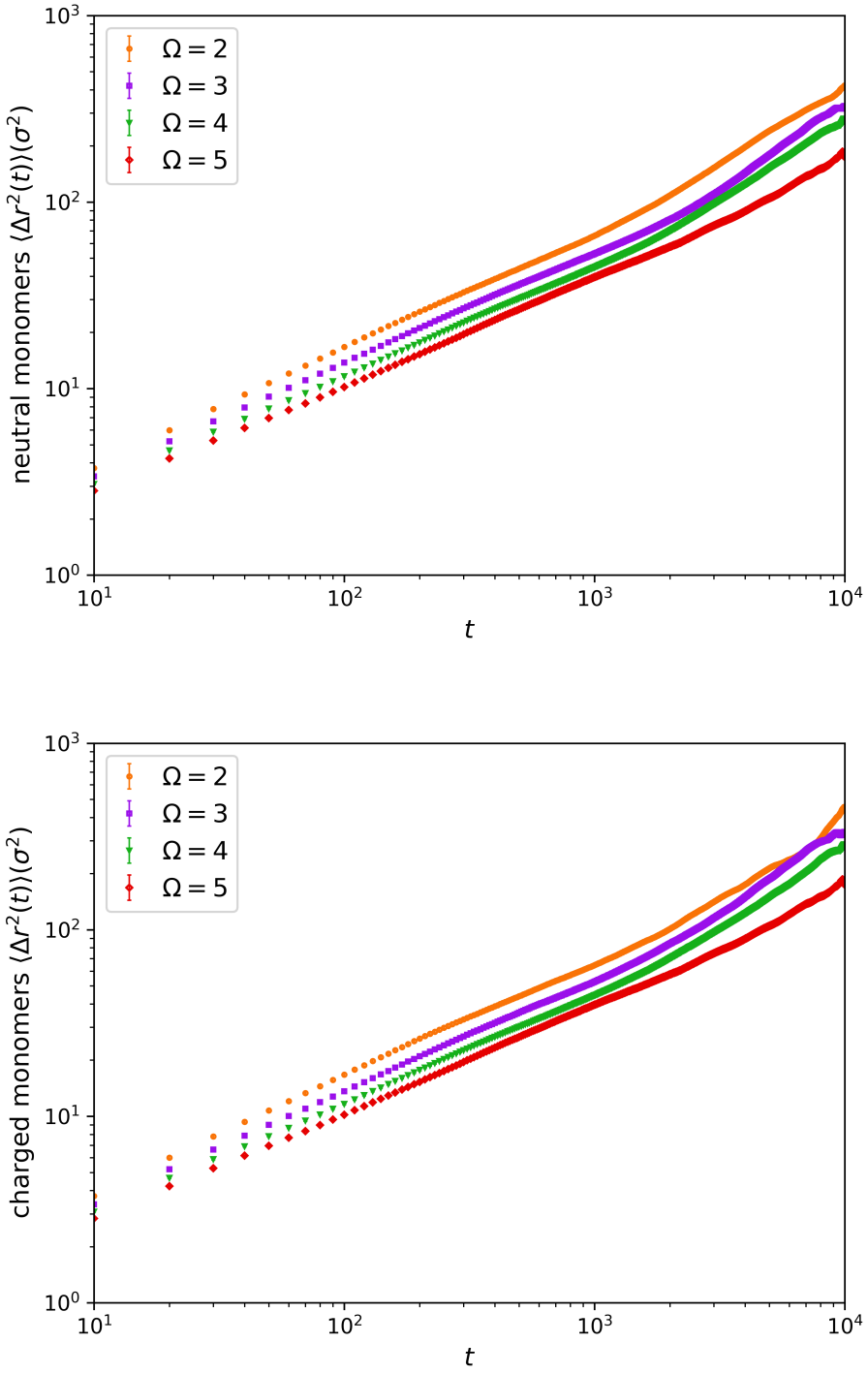

Figure S15: MSD as a function of Ω for neutral (upper panel) and charged (lower panel) monomers.

Trajectory Movies

We provide the following trajectory movies for systems at the free–swelling equilibrium:

- S1_full_system_omega2.mp4
- S2_full_system_omega3.mp4
- S3_full_system_omega4.mp4
- S4_full_system_omega5.mp4
- S6_detail_omega3.mp4
- S7_detail_omega4.mp4
- S8_detail_omega5.mp4

"Full system" movies show the entire box cell with periodic replicas in some direction; here, the diameter of all monomers has been reduced by roughly one half with respect to the real one. In "detail" movies, instead, a few interacting stars are shown, while the other polyelectrolytes in the box are not visible.